Journal of Materials Chemistry A

REVIEW

View Article Online
View Journal | View Issue

Cite this: J. Mater. Chem. A, 2016, 4, 17623

Doping and alloying for improved perovskite solar cells

Yuanyuan Zhou,†[a] Zhongmin Zhou,†[b] Min Chen,[a] Yingxia Zong,[ab] Jinsong Huang,[c] Shuping Pang[b] and Nitin P. Padture*[a]

Received 7th October 2016
Accepted 27th October 2016

DOI: 10.1039/c6ta08699c

www.rsc.org/MaterialsA

Doping and/or alloying in the various layers in perovskite solar cells (PSCs) is playing a key role in the success of this new photovoltaic (PV) technology. Here we present a brief review of doping and alloying approaches used to enhance the efficacy of the hybrid organic–inorganic perovskite (HOIP) layer, the electron-transporting layer (ETL), the hole-transporting layer (HTL), and the electrode layers in PSCs. While the effectiveness of these approaches is beyond doubt, the fundamental understanding of doping and alloying in the majority of the cases is lacking. This presents vast research opportunities in elucidating the roles of doping and alloying, and the rational design and implementation of these approaches for enhanced PSCs performance.

1. Introduction

We are witnessing the emergence of perovskite solar cells (PSCs) as a new generation photovoltaic (PV) technology,[1–6] where the power conversion efficiency (PCEs) of PSCs have shot up to >22% in an unprecedentedly short period of time of seven years.[1] PSCs employ a group of hybrid organic–inorganic perovskite (HOIP) materials as light absorbers, with the general formula of ABX_3 (see Fig. 1), where A = $CH_3NH_3^+$ (methylammonium or MA^+), $HC(NH_2)_2^+$ (formamidinium or FA^+), or Cs^+; B = Pb^{2+} or Sn^{2+}; and X = I^-, Br^-, or Cl^-.[6–8] Amongst these compounds, methylammonium lead triiodide ($CH_3NH_3PbI_3$ or $MAPbI_3$) HOIP is the most widely studied composition. Although the synthesis and basic properties of $MAPbI_3$ were studied in the early 1990s,[9] Kojima *et al.*[2] were the first to demonstrate the use of the $MAPbI_3$ as the 'dye' in liquid-junction PSCs, a derivative of dye-sensitized solar cells (DSSCs). However, the performance of such liquid-junction PSCs degraded rapidly due to the dissolution of these HOIP 'dyes' in the liquid electrolyte.[10] In order to resolve this issue, in 2012, Kim *et al.*[10] replaced the liquid electrolyte with solid-state hole-transporting materials, and fabricated all-solid-state PSCs with PCEs up to 9.3%. In parallel, Lee *et al.*[3] invented a novel mesosuperstructured solar cell, where an insulating mesoporous Al_2O_3 scaffold was used to replace the conventional electron-transporting mesoporous TiO_2 scaffold. A surprising 10.2% PCE was achieved in these PSCs.[3] This invention eventually led to the emergence of planar-structured PSCs, as the insulating mesoporous Al_2O_3 layer did not appear to play an actual role in the solar cell operation.[5] To date, extensive effort has gone into optimizing the solar cell structure,[11,12] and it appears that the mesoscopic–planar hybrid PSC with both a mesoporous TiO_2/HOIP composite layer and a planar HOIP capping layer is the most efficient embodiment, as it combines the merits of both mesoscopic and planar-junction PSCs.[13,14]

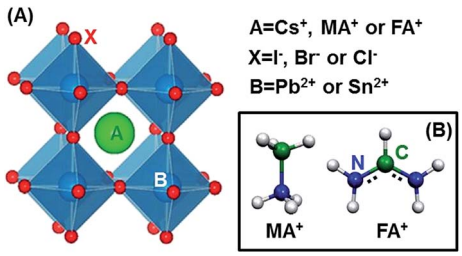

Fig. 1 (A) Schematic crystal structure of HOIPs with typical A, B, and X site ions. (B) Methylammonium (MA) and formamidinium (FA) molecular cations.

While optimization of PSCs architecture has played a key role in the early stages of PSCs development, there has been a surge of interest in the compositional tailoring of the PSC device components, which is expected to further the advance of PSCs technology in terms of PCE, stability, toxicity, *etc.* As seen in Fig. 2, a typical PSC consists of a HOIP absorber layer, an electron-transporting layer (ETL), a hole-transporting layer (HTL), and the electrode contacts.[15] Under illumination, the light is absorbed by the HOIP layer, where charge carriers (electrons and holes) are generated. These photo-generated

[a]School of Engineering, Brown University, 184 Hope Street, Providence, Rhode Island 02912, USA. E-mail: nitin_padture@brown.edu

[b]Qingdao Institute of Bioenergy and Bioprocess Technology, Chinese Academy of Sciences, 189 Songling Road, Qingdao 266101, P. R. China

[c]Department of Mechanical and Materials Engineering, University of Nebraska, Lincoln, Nebraska 68588, USA

† These authors contributed equally.

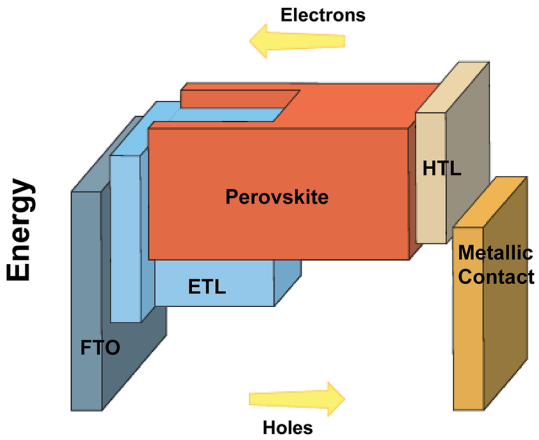

Fig. 2 Schematic illustration of the energy levels of the various layers in a typical PSC (reprinted with permission from ref. 15).

electrons and holes are extracted and transported in the ETL and HTL, respectively, and collected by the electrodes. The PSC is usually regarded as a simple p–i–n cell with high quality intrinsic HOIP absorber layer,[16] although a recent detailed study[17] has revealed that the p–n junction structure at the HOIP/TiO_2 interfaces is the dominant feature in the most popular PSCs with TiO_2 ETLs. While the exact working principle is still being debated, there is no doubt that the overall performance of PSCs is the result of the harmonious operation of all these layers (HOIP, ETL, HTL, and electrodes), making the physical/chemical properties of all these layers, and the interfaces, critically important.

In this context, compositions of each of the PSC layers *via* doping and/or alloying are engineered in order to maximize the overall performance of PSCs, which forms the basis for this review article. First of all, it is important to define the terms 'doping' and 'alloying' from a materials science perspective. Doping is regarded as intentional introduction of a small amount of 'impurities' into an otherwise pure material (host) to tune its electronic properties (*e.g.* hole or electron transport).[18–21] Alloying is the formation of solid solution of two or more materials.[18,19,22] Thus, in doping, the concentration is usually very low, compared to alloying, and doping does not change the crystal structure of the host material. Also, generally doping is aimed at improving certain properties without altering the basic characteristics of the host material, whereas new materials with new properties can be produced in the case of alloying.[19] (It is important to note that, for solution-processed PSCs, all the reported compositions in the literature usually refer to the percentage of constituent elements in the precursor solution, rather than the actual compositions in the solid films which can be difficult to determine.)

2. Alloying and doping in ABX_3 HOIPs

As per the above criteria for distinguishing doping and alloying, most studies in the literature in the area of compositional tailoring of the HOIP absorbers are focused on alloying, where alloys can be formed by substituting A, B, and X sites with their corresponding elemental or molecular analogues in the ABX_3 perovskite crystal structure.

2.1. A-site alloying in ABX_3 HOIPs

The most popular $MAPbI_3$ HOIP has a bandgap of ~1.55 eV.[2–4] To further reduce the bandgap, the FA^+ cation (ionic radius: ~2.2 Å),[23] which is slightly larger than the MA^+ cation (ionic radius: ~1.8 Å),[23] can be incorporated into the $MAPbI_3$ perovskite structure, forming mixed-organic-cation HOIP alloys $MA_xFA_{1-x}PbI_3$ (x ranging from 0 to 1) with extended absorption into the near-infrared (IR) region of the solar spectrum (Fig. 3A). Pellet *et al.*[24] were the first to investigate the properties and performance of the $MA_xFA_{1-x}PbI_3$ HOIP alloys in mesoscopic PSCs. In that study, $MA_xFA_{1-x}PbI_3$ HOIPs were formed *via* the classic 'dipping' reaction of pre-deposited PbI_2 mesoscopic films with the tailored $MA_xFA_{1-x}I$ solution in isopropanol.[24] They showed that the $MA_{0.6}FA_{0.4}PbI_3$ composition alloy exhibited the best overall PSC performance (Fig. 3B), with an extended absorption edge at ~810 nm, which is close to that of pure $FAPbI_3$ HOIP.[24] Several later studies have implied that the superior performance of PSCs based on $MA_xFA_{1-x}PbI_3$ alloys compared to pure $FAPbI_3$ may also be related to the phase instability of pure $FAPbI_3$ HOIP in the ambient.[13,25] In fact, $FAPbI_3$ has two possible polymorphs[23–30] at room temperature, the 'black' perovskite phase (α-$FAPbI_3$, space group $P3m1$ [ref. 26] or $Pm\bar{3}m$ [ref. 31]), and the 'yellow' non-perovskite phase (δ-$FAPbI_3$, space group $P6_3mc$ [ref. 26]). In the ambient, the 'yellow' δ-$FAPbI_3$ can form easily *via* a facile α → δ phase transition[29] or as a byproduct associated with the crystallization of the $FAPbI_3$ HOIP.[28,30] However, interestingly, the incorporation of MA^+ into the $FAPbI_3$ perovskite structure results in much more stable HOIP phases. This idea was first proposed by Jeon *et al.*[13] who prepared stable PSCs based on $(MAPbBr_3)_{0.15}$-$(FAPbI_3)_{0.85}$ HOIP composition, and achieved a record (at that time) certified PCE of 16.2%. Regardless of the additional Br alloying (discussed below) in that work, the alloying of MA^+ and FA^+ is expected to play a major role in stabilizing the perovskite phase, which was further studied by Binek *et al.*[25] As shown in Fig. 3C and 3D, incorporation of MA^+ cation favors the solution crystallization of high-purity perovskite phases. It is hypothesized that the higher dipole of MA^+ cation has stronger interaction with the $[PbI_6]$ octahedral cage, which stabilizes the perovskite structure as shown in Fig. 3E. Owing to the combined merits of extended absorption and enhanced ambient stability, $MA_xFA_{1-x}PbI_3$ HOIP alloys have been studied extensively,[32–34] and various fabrication techniques have been developed in order to realize their full potential in PSCs. For example, Liu *et al.*[33] prepared high-quality $MA_xFA_{1-x}PbI_3$ HOIP thin films *via* a two-step reaction of MAI with an $(FAI)_{1-x}PbI_2$ intermediate complex. Deng *et al.*[34] developed a 'doctor-blading' process for scalable deposition of $MA_xFA_{1-x}PbI_3$ HOIP thin films. High performance and stability in the resulting PSCs were achieved, which are attributed to the intrinsic merits and improved grain morphologies of $MA_xFA_{1-x}PbI_3$ HOIP alloys.[32–34]

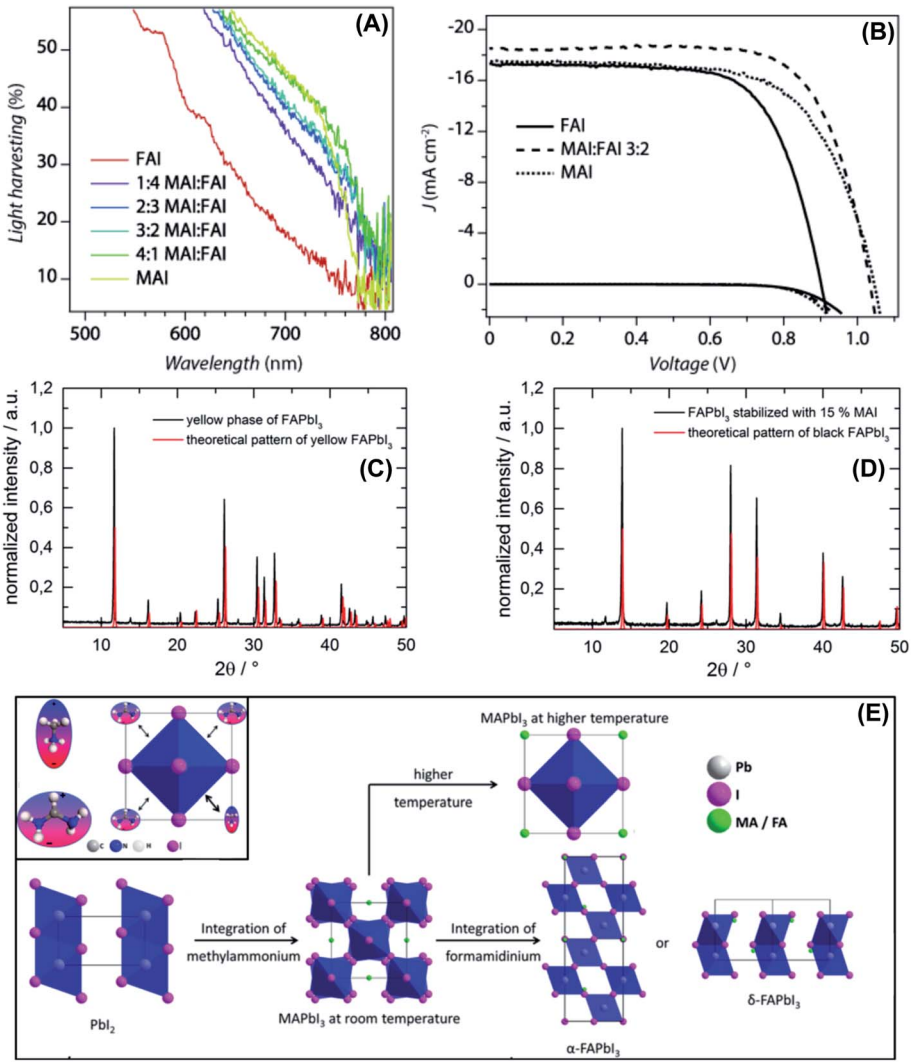

Fig. 3 (A) UV-vis absorption spectra of mixed FA–MA HOIP thin films with different compositions (reprinted with permission from ref. 24). (B) Comparison of *J*–*V* curves of PSCs based on $MAPbI_3$, $MA_{0.6}FA_{0.4}PbI_3$, and $FAPbI_3$ HOIPs (reprinted with permission from ref. 24). XRD patterns of: (C) the yellow δ-$FAPbI_3$ phase and the (D) the $MA_{0.15}FA_{0.85}PbI_3$ HOIP phase (reprinted with permission from ref. 25). (E) Schematic illustration of the stabilization mechanism of the α-$FAPbI_3$ HOIP phase *via* MA^+ alloying (reprinted with permission from ref. 25).

Similar to MA^+, elemental Cs^+ cation (ionic radius: 1.67 Å)[35–37] has also shown exceptional promise as an A-site alloying candidate for stabilizing $FAPbI_3$ perovskite. Lee *et al.*[35] first reported $Cs_xFA_{1-x}PbI_3$ HOIP alloys and hypothesized that the substitution of FA^+ by Cs^+ induces the contraction of the cubo-octahedral volume, and thereby enhances (FA–I) interaction, which stabilizes the perovskite structure. They showed that substitution of 10% of FA^+ cations by Cs^+ enhances the photo-stability and the moisture-tolerance of the PSCs significantly, while increasing the PCE from 14.9% to 16.5%. A similar observation was later reported by Yi *et al.*,[36] where they performed first-principles calculations to elucidate such remarkable stabilization behavior. As shown in Fig. 4, the entropic gains, together with the small internal energy input, favor the formation of α-phase $Cs_xFA_{1-x}PbI_3$ compounds with a stable perovskite structure over the δ-phase. The enhanced stability of $Cs_xFA_{1-x}PbI_3$ HOIPs was also explained by Li *et al.*[37] using empirical Goldschmidt tolerance factor (*t*) considerations. It was shown that the calculated *t* for $FAPbI_3$ is $t > 1$, while $t < 0.8$ for $CsPbI_3$. Through alloying of large-*t* $FAPbI_3$ and small-*t* $CsPbI_3$, *t* can be tuned to between 0.8 and 1.0 in $Cs_xFA_{1-x}PbI_3$ compounds, which favors their existence in stable perovskite structure. However, although these studies have claimed the successful alloying of Cs^+ and FA^+ in the perovskite structure, it is not clear whether Cs^+ is indeed incorporated into the perovskite crystal structure. Thus, the unambiguous determination of the exact location of Cs^+ in $Cs_xFA_{1-x}PbI_3$ HOIPs would be very important for understanding the underlying mechanism of Cs^+–FA^+ alloying-induced phase stabilization.

2.2. B-site alloying in ABX_3 HOIPs

B-site alloying is primarily adopted to address the toxicity of HOIP materials. To date, the most efficient PSCs employ lead (Pb)-based HOIPs ($FAPbI_3$, $MAPbI_3$, *etc.*) that contain

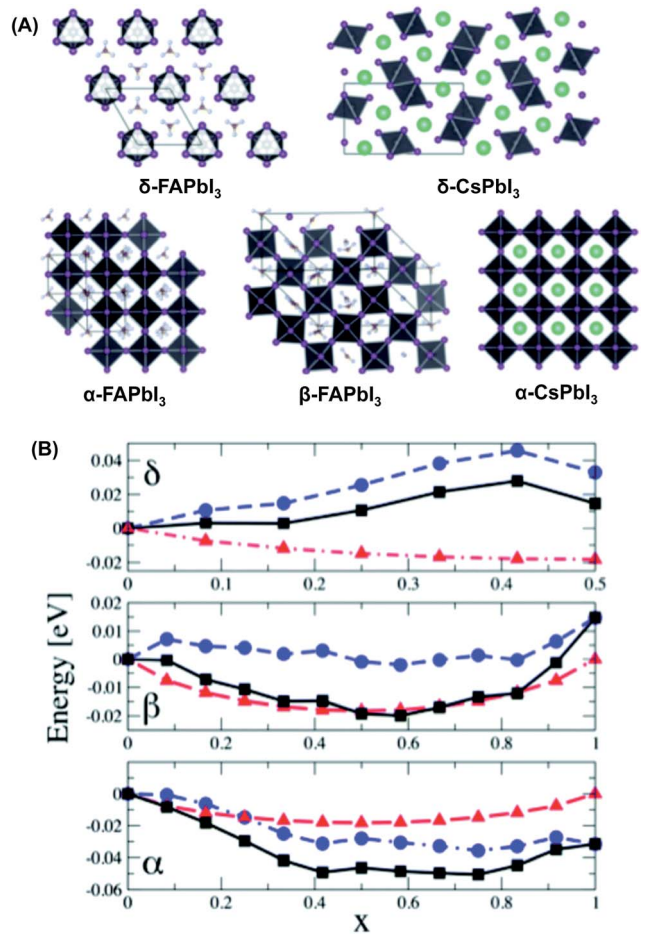

Fig. 4 (A) Crystal structures of various polymorphs of $CsPbI_3$ and $FAPbI_3$ (reprinted with permission for ref. 36). (B) Relative energy gains for the formation of α-, β-, and δ-phase $Cs_xFA_{1-x}PbI_3$ (reprinted with permission for ref. 36).

a significant fraction (>30 wt%) of Pb.[38] This raises toxicity concerns for manufacturing, deployment, and disposal of future PSCs. To address this issue, tin (Sn), as an elemental analogue of Pb, is chosen to replace the Pb in HOIPs.[39,40] However, several studies have shown that the use of $MASnI_3$ light absorbers in PSCs results in significantly inferior performance (<10% PCEs) compared to Pb-based PSCs, primarily due to the metallic nature of $MASnI_3$.[39,40] In this context, an interesting strategy is to use $MAPb_xSn_{1-x}I_3$ alloys to reduce the amount of Pb contained within PSCs, while maintaining high PSC performance.[41,42] It is also worth noting that, while Sn is less toxic than Pb, Babayigit *et al.*[43,44] have shown that the strong acidification of Sn-based perovskites can also cause environmental concerns.

In this context, Stoumpos *et al.*[26] experimentally confirmed that $MAPb_xSn_{1-x}I_3$ HOIP alloys with the 3D perovskite structure can form a mixture of $MAPbI_3$ and $MASnI_3$ *via* either solid reaction or solution synthesis. Changing the x value results in the tuning of the optical absorption of these HOPIs, as shown in Fig. 5A.[41] Interestingly, as seen in Fig. 5B, the bandgap change with x does not follow a linear trend (Vegard's law) in $MAPb_xSn_{1-x}I_3$, but instead an anomalous bandgap behavior is observed.[41] It appears that a HOIP composition of $MAPb_{0.5}Sn_{0.5}I_3$ prepared from solution route has the lowest bandgap of 1.17 eV, compared to 1.55 eV for $MAPbI_3$, and 1.30 eV for $MASnI_3$. PSCs using $MAPb_{0.5}Sn_{0.5}I_3$ HOIP as the light absorber were also reported by Hao *et al.*[41] and Ogomi *et al.*[42] The edges of the external quantum efficiency (EQE) spectra from these PSCs were found to extend to 1060 nm wavelength, owing to the optimized bandgap. However, in contrast to the experimental observations, density functional theory (DFT) calculations by Ju *et al.*[45] and by Mosconi *et al.*[46] have revealed that the calculated bandgaps of $MAPb_xSn_{1-x}I_3$ HOIPs are proportional to the x value. Such inconsistency between experiment and theory could be due to the variation in the real crystal symmetry of perovskites with different x values. Note that the crystal structure of pure $MAPbI_3$ perovskite is tetragonal (space group $I4/mcm$), whereas that of pure $MASnI_3$ is cubic (space group $Pm\bar{3}m$) at room temperature.[19] Therefore, more careful analyses of the crystal structures of $MAPb_xSn_{1-x}I_3$ HOIP alloys, and more refined theoretical models, are needed to elucidate the origin of this anomalous bandgap behavior. Nevertheless, in the case of $MAPb_xSn_{1-x}Br_3$, Mancini *et al.*[47] indeed observed a linear trend of the bandgap, with increasing Sn content, from 2.20 eV ($x = 0$) to 1.33 eV ($x = 1$), which can be related to the fact that $MAPbBr_3$ and $MASnBr_3$ exhibit the same cubic symmetry. In addition to the bandgap-tuning effect, DFT calculations by Mosconi *et al.*[46] also revealed that mixed Sn–Pb HOIP alloys show more balanced electron and hole effective-mass values compared to single-metal-cation HOIPs. In this regard, although PCEs of PSCs based on Pb–Sn HOIP alloys are still lower than those based on Pb alone, these alloys are promising for their reduced toxicity and extended absorption, as well as enhanced charge-transport properties.

2.3. X-site alloying in ABX_3 HOIPs

Since the halogen ion plays a profound role in determining the bandgap of halide HOIPs,[48,49] alloying of smaller cation halides (Br^-) into lead iodide HOIPs ($MAPbI_3$, $MASnI_3$, $FAPbI_3$, *etc.*) allows bandgap tuning in a wide range of 1.45 to 2.3 eV. Since the time Noh *et al.*[50] investigated the application of mixed I–Br HOIPs ($MAPbI_{3-x}Br_x$) for enabling the color management of PSCs (Fig. 6A and B), several studies on the crystallization and physical properties (photovoltaic, luminescent, *etc.*) of these HOIPs have been reported. In particular, $MAPbI_{3-x}Br_x$ (x = 0.6–1.0) HOIPs have bandgaps of 1.7–1.8 eV, which hold unprecedented promise in the application as top-cell, in conjunction with low-bandgap inorganic bottom-cell based on crystalline Si or copper–indium–gallium–selenide (CIGS), in tandem devices.[51,52] However, it is been shown that these $MAPbI_{3-x}Br_x$ ($x > 0.6$) HOIPs show phase segregation under illumination, resulting in the formation of I-rich and Br-rich regions.[53] Such photo-induced phase segregation behavior may limit the performance of the corresponding PSCs, as the open-circuit voltage (V_{OC}) can be pinned by the segregated I-rich phase. Also, a randomly distributed low-bandgap phase in the film acts as charge traps that reduce the photocurrent in PSCs. Similar photo-instability issue may occur in the $FAPbI_{3-x}Br_x$ as

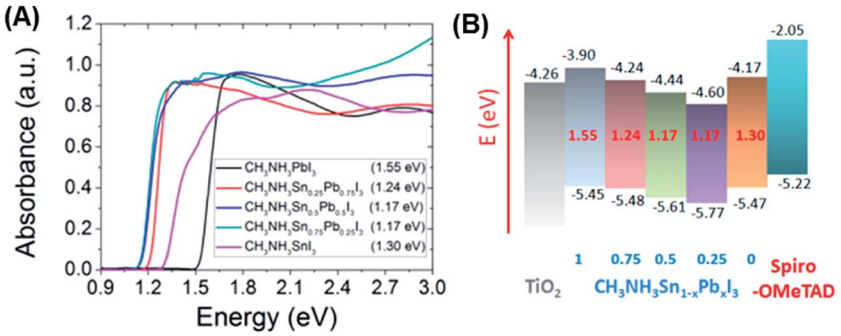

Fig. 5 (A) Absorption spectra of $MAPb_xSn_{1-x}I_3$ thin films (reprinted with permission for ref. 41). (B) Energy levels (valence band maximum, conduction band minimum) of $MAPb_xSn_{1-x}I_3$ HOIPs, compared to TiO_2 and Spiro-OMeTAD (reprinted with permission for ref. 41).

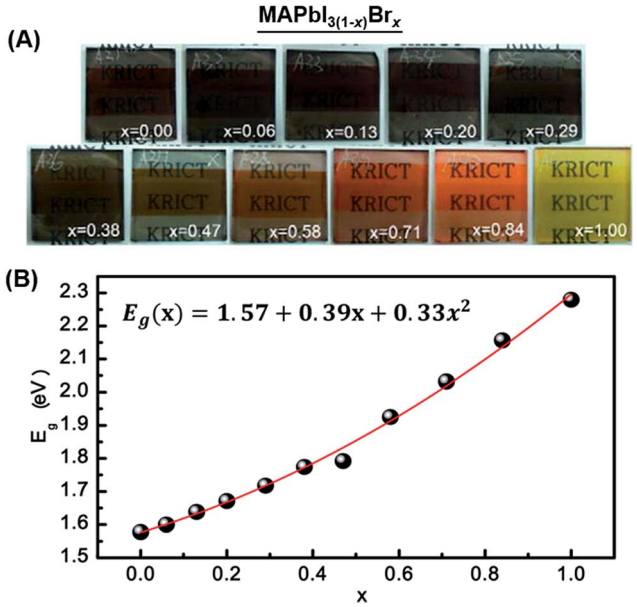

Fig. 6 (A) Photographs of $MAPb(I_{1-x}Br_x)_3$ HOIP alloy thin films with different x values (reprinted with permission for ref. 50). (B) Variation of bandgap (E_g) of $MAPb(I_{1-x}Br_x)_3$ HOIP thin films as a function of x (reprinted with permission for ref. 50).

well.[54] Furthermore, it is claimed that partial substitution of I^- with Br^- may enhance the moisture tolerance of mixed-halide HOIPs.[50] However, in a contradicting report it was shown that the introduction of Br^- actually stresses the perovskite structure and accelerates its degradation.[55] Besides Br^-, Cl^- has also been suggested as an alloying anion for $MAPbI_3$ HOIP in the early stage of PSCs development,[3] but, this issue is still controversial, which is discussed in Section 2.5.

2.4. Dual-site or triple-site alloying in ABX_3 HOIPs

As discussed above, A-, B-, and X-site alloying strategies are generally adopted for improving different aspects of PSCs. Thus, it is possible to combine two or three of them simultaneously in order to achieve multiple goals. For example, as mentioned earlier, the photo-stability of the promising mixed-halide HOIP alloys ($MAPbI_{3-x}Br_x$ or $FAPbI_{3-x}Br_x$) is a concern, and, therefore, further A-site alloying is adopted to alleviate this issue. It appears that such dual-site compositional engineering could lead to the formation of stable mixed-halide HOIPs with continuous bandgaps/colors, as seen in Fig. 7A and 7B. McMeekin *et al.*[54] showed that the photoluminescence (PL) emission of the dual-site perovskite alloy $FA_{0.83}Cs_{0.17}PbI_{1.8}Br_{1.2}$ HOIP thin films does not red-shift under monochromatic irradiance of much higher irradiance of 5 W cm^{-2} after 240 seconds, whereas obvious red-shift is observed in thin films made of neat FA-based mixed-halide HOIPs (Fig. 7C). Furthermore, elemental substitution at each site in ABX_3 structure may have a combined effect on the intrinsic properties as well as the crystallization process of the HIOP materials. In this context, there is a clear trend towards using these dual-site HOIP alloys with more complicated compositions (*e.g.* $FA_{0.85}MA_{0.15}PbI_{2.55}Br_{0.45}$ [ref. 13 and 56–58], $Cs_x(MA_{0.17}FA_{0.83})_{(1-x)}Pb(I_{0.83}Br_{0.17})_3$ [ref. 59], $FA_xMA_{1-x}Pb(I_{1-y}Br_y)_3$ [ref. 60]) in the PSCs to achieve maximum PSC performance. However, the reasons why these particular compositions result in the enhancement in the PSC performance are far from well-understood, which can be an important subject for future research in PSCs. Also, although a HOIP alloy with simultaneously mixed compositions at all the three sites (A, B, and X) has not been reported, such triple-site alloys might open up new opportunities for higher-performance PSCs.

2.5. Doping in ABX_3 HOIPs

Compared with the extensive studies on alloying of HOIPs, there have been relatively fewer studies on doping of HOIP, and they appear to be more controversial. One of the most popular topics still under debate is the effect of chlorine (Cl). In 2012, Lee *et al.*[3] reported that the mixed-halide HOIP '$MAPbI_2Cl$' is an efficient light absorber in PSCs. But later on, it was recognized that single-phase '$MAPbI_2Cl$' alloy does not exist, and, thus, the '$MAPbI_{3-x}Cl_x$' nomenclature was adopted as the value of x is not known.[61] One hypothesis is that Cl^- may work as a dopant with very little concentration in $MAPbI_3$, which can only be detected by high-resolution analytical characterization tools.[62–64] However, Cl^- has been found to play a significant role in the solution crystallization and grain growth of $MAPbI_3$.[65–67] Thus, it still is a mystery whether the slight amount of remnant Cl^- in

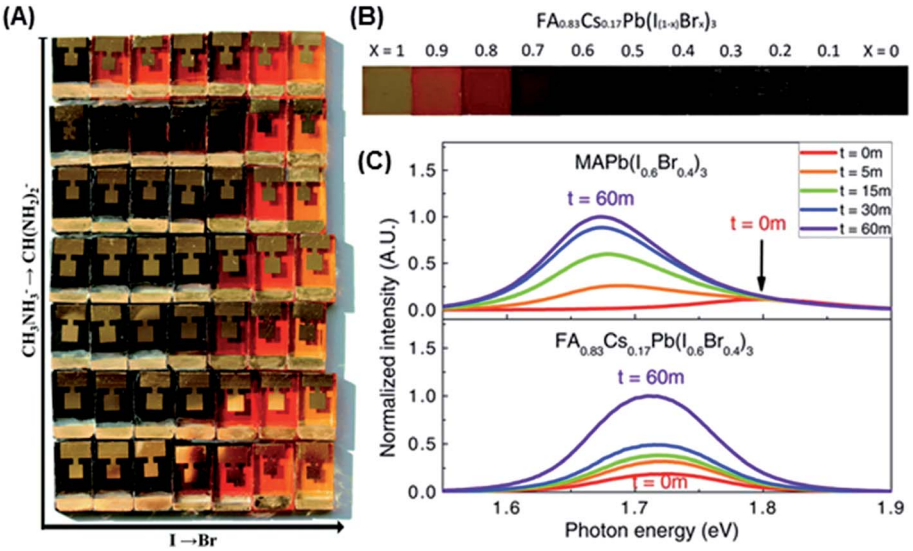

Fig. 7 Photographs of perovskite solar cells using: (A) $FA_xMA_{1-x}Pb(I_{1-y}Br_y)_3$ absorbers with different x and y values, and (B) $FA_{0.83}Cs_{0.17}Pb(I_{1-x}Br_x)_3$ absorbers with different x values (reprinted with permission from ref. 60). (C) Evolution of PL emissions of $MAPb(I_{0.6}Br_{0.4})_3$ and $FA_{0.83}Cs_{0.17}Pb(I_{0.6}Br_{0.4})_3$ HOIP alloys as a function of laser excitation time (reprinted with permission from ref. 54).

the film is doping the crystal lattice of $MAPbI_3$ or whether the enhancement of the film quality is related to the presence of Cl^-.[65–67] Similar controversies may exist in other reported 'doped' HOIPs, as detailed characterization of the location and the concentration of the dopants at the atomistic scale is missing. Nevertheless, several groups have reported the enhancement of the performance of HOIPs in PSCs with the addition of various elemental components (*e.g.* heterovalent cations[68] and molecular ions[69,70]). Abdi-Jalebi *et al.*[71] explored possible doping by monovalent cations with ionic radii similar to that of Pb^{2+} (*e.g.* Cu^+, Na^+, *etc.*), where they concluded that such doping has significant effect on the absorption and hole motilities compared to undoped $MAPbI_3$ HOIP. Abdelhady *et al.*[68] reported trivalent-dopant incorporation in HOIP crystals and achieved four orders-of-magnitude enhancement in the electrical conductivity, and a change in the sign of majority charge carriers *via* Bi^{3+} incorporation. Another type of popular proposed dopants is molecular ions. Mei *et al.*[72] and Chen *et al.*,[69] respectively, reported doping of amino-acid cation and BF_4^- anion for the enhancement of electronic properties and photovoltaic performance of HOIPs in HTL-free mesoscopic PSCs. Pseudohalide cations such as SCN^- are also studied as possible dopant candidates for HOIPs.[70,73] But, again, the exact roles of these proposed 'dopants' need to be further elucidated and separated, as the effect of these 'dopants' in the solution crystallization of HOIPs can be usually profound.[74] Furthermore, there is no available information indicating that the reported doping in the HOIP is either p-type or n-type. Meanwhile, it is interesting that Yin *et al.*[75] and Wang *et al.*[76] showed experimentally and theoretically, respectively, that HOIPs may be possibly self-doped as a result of the manipulation of crystal defects.

3. Doping in ETLs

ETLs in PSCs are broadly classified into two categories: inorganic and organic. TiO_2 and C61-butyric acid methyl ester (PCBM) are the most commonly used inorganic and organic ETLs, respectively.[77] Neat ETL materials are limited in their electron-transporting characteristics (electron mobility and conductivity) due to their polycrystalline or semi-crystalline nature. In particular, TiO_2 ETL materials synthesized at low temperatures have even poorer electronic properties. In this context, incorporation of dopants or additives into TiO_2 and PCBM becomes necessary to match the excellent electronic properties of HOIP absorber materials[78] in order to optimize the PSC performance.

3.1. Doping in TiO_2 ETLs

Doping of TiO_2 ETLs (which also includes the TiO_2 mesoporous layer) has been studied extensively in the context of DSSCs.[79–82] In TiO_2, both cationic and anionic dopants can be used. The former are mostly metals (Li, Mg, Zr, Nb, *etc.*) whereas the latter are non-metals (C, N, *etc.*).[79] Cationic dopants are expected to affect the conduction band (CB) and the valence band (VB), whereas anionic dopants are expected to influence the Fermi level (E_F), with profound impact on the electron injection/transport in the PSC devices. The mechanisms of doping in TiO_2 have been reviewed extensively by Roose *et al.*,[79] and is summarized here. As shown in Fig. 8A, in pristine TiO_2, electrons are transported by hopping from one shallow trap to another shallow trap.[79] The shallow-trap density influences electron transport rate, and, thus, the short-circuit current density (J_{SC}) in solar cells.[79] But, deep traps can trap electrons permanently, and act as recombination sites, affecting V_{OC}.[79] In some cases, doping decreases the deep-traps density and results

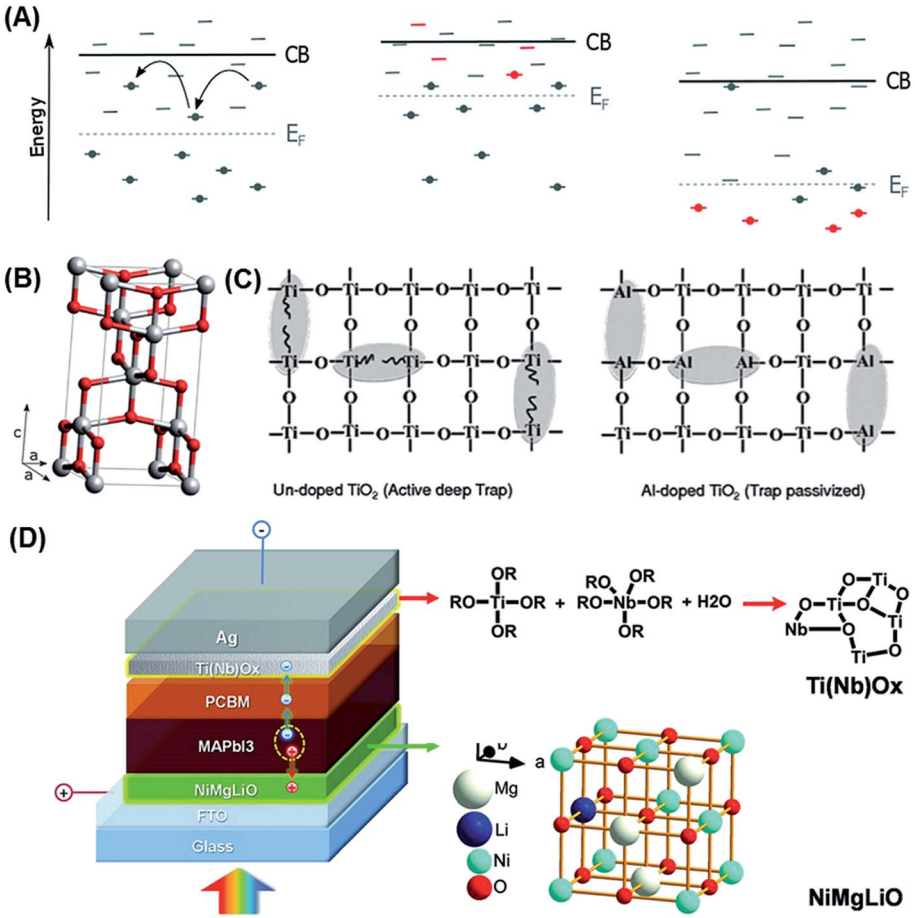

Fig. 8 (A) Schematic illustration showing the effect of doping on the CB and E_F of TiO_2. The doping-induced states are shown in red. Left: In pristine TiO_2, electrons are transported by 'hopping' from one shallow trap to another shallow trap. Center: In some cases, doping decreases the deep trap density and results in an upward shift of E_F and conduction band. Right: In some other cases, doping contributes to the formation of deep traps, resulted into the downward shift of the CB and E_F (reprinted with permission from ref. 79). (B) The anatase TiO_2 unit cell, with Ti atoms in grey and O atoms in red (reprinted with permission from ref. 79). (C) Schematic illustration of Al-doping in TiO_2 for passivation of deep traps (reprinted with permission from ref. 90). (D) Schematic illustration of a PSC using Nb-doped TiO_2 ETL and (Mg, Li)-doped NiO HTL (reprinted with permission from ref. 89).

in an upward shift of E_F, both of which contribute to an increase in V_{OC}.[79] Note that V_{OC} is also defined as the difference between E_F of TiO_2 and the HTL. However, since CB also shifts towards lowest unoccupied molecular orbitals (LUMO) of the absorber, the driving force for electron injection is lowered. This combined with a decreased trap density, and the related electron transport, lowers J_{SC}.[79] In some other cases, doping contributes to the formation of deep traps, shifting CB and E_F downwards, which causes a decrease in V_{OC}.[79] However, the larger offset between TiO_2-CB and absorber-LUMO, and the higher trap density, enhances electron injection and transport, respectively, which leads to enhanced J_{SC}.[79] In this context, a dopant for TiO_2 that eliminates deep traps, and simultaneously introduces new states close to CB, is expected to enhance both V_{OC} and J_{SC} of PSCs.[79]

Enormous research effort in doping TiO_2 has gone towards improving the performance of DSSCs. However, since PSCs are still in a relatively early stage of development, majority of the research effort is focused on improving the morphological and electronic properties of the HOIP layer. Nevertheless, it appears that the highest-PCE PSCs rely on a TiO_2 ETL, and, thus, their engineering *via* doping is an important topic for future research. Some studies on doping of TiO_2 ETLs have been reported in the literature, and superior performance of PSCs based on doped-TiO_2 has been demonstrated in various aspects (electron injection/transport, hysteresis, and stability).[83–89]

For improving electron transport in PSCs, Zhou *et al.*[88] have shown that the conductivity of low-temperature solution-processed Y-doped TiO_2 ETL increases from 0.6×10^{-5} S cm^{-1} to 2×10^{-5} S cm^{-1} (four-point conductivity measurements). The series resistance in the corresponding PSC device also reduced from 9.12 Ω to 5.34 Ω.[88] In another study, Chen *et al.*[89] found that the conductivity of TiO_2 ETL increased from $\sim 10^{-6}$ S cm^{-1} to $\sim 10^{-5}$ S cm^{-1} upon the addition of 5 mol% Nb to the TiO_2 precursor solution (scanning-probe-microscopy measurements). These results indicate that Nb can partially reduce Ti^{4+} to Ti^{3+} within the TiO_2 crystal structure, which passivates the electronic defect states, enabling fast electron transport. Fig. 8D

shows the typical PSC structure made by Chen *et al.*[89] using a Nb-doped TiO_x ETL, where the PCE of PSC reached >15% (certified), for the first time, in an active cell area >1 cm^2, with doping playing a key role.

Doping in TiO_2 can also alleviate hysteresis and stability issues in PSCs using TiO_2 ETLs; it has been suggested that this is related to the intrinsic oxygen vacancies in the anatase TiO_2 (Fig. 8B). The oxygen vacancies can act as deep trap states in TiO_2. Through incorporation of dopants such as Al^{3+}, these trap states can be effectively reduced as shown in Fig. 8C, ameliorating the PSC degradation issue.[90] Nagaoka *et al.*[91] and Giordano *et al.*[92] showed that the hysteresis of PSCs is also significantly reduced by passivation of TiO_2 surface traps *via* cationic doping.

Doping in TiO_2 ETLs may have other non-electronic effects in the PSCs. For example, it is observed that Y-doping also affects the surface properties of TiO_2, which improves the crystallization of HOIPs on top of the TiO_2.[93] Overall, there are vast research opportunities in studying doping effect in TiO_2 for PSCs and understanding the underlying mechanisms, as well as developing effective doping strategies in TiO_2 *via* various synthetic routes. It is expected that the lessons learned from DSSCs research in the past two decades in this area will have significant impact on the progress of PSCs.

3.2. Doping in fullerene ETLs

The basic mechanism of doping in organic materials is similar to that in inorganic semiconductors (*e.g.* TiO_2). As shown in Fig. 9A, dopants are needed to donate electrons to LUMO states or extract holes from highest occupied molecular orbital (HOMO) states to achieve n or p doping, respectively. However, compared to doping in inorganic materials, insights into the doping of organic semiconductors are far less developed, which is due to the fact that the widely used hydrogen model for inorganic semiconductors does not work for organic semiconductors.[86] Nevertheless, the past studies have established various empirical doping rules in the field of organic PVs, which can be adopted for the development of PSCs.[94–97]

To enhance the electrical properties of the fullerene ETLs, Kim *et al.*[98] reported 1,3-dimethyl-2-phenyl-2,3-dihydro-1*H*-benzoimidazole (DMBI) as an effective n-dopant. They showed that the electrical conductivity of the DMBI-doped PCBM film (6.1×10^{-5} S cm^{-1}) is four orders-of-magnitude higher than that of the pristine PCBM film (3.8×10^{-9} S cm^{-1}), and the E_F level up-shifts after DMBI-doping. Correspondingly, PSCs using DMBI-doped PCBM exhibit higher PCEs with remarkably higher J_{SC}. Similarly, Kuang *et al.*[99] introduced graphdiyne (GD) into the PCBM layer in PSCs, which enhances the electrical conductivity, electron mobility, and charge extraction ability in the ETL layer, owing to the delocalized π-systems of GD material (shown schematically in Fig. 9B). The corresponding PSCs has a ~30% increase in overall PCEs (from 10.8% to 13.9%) after GD 'doping'. Another interesting study by Bai *et al.*[100] showed that MAI, an ingredient in the HOIP solution precursor, could be also serve as a good dopant for PCBM, since the halide ions are good electron donors.

It is noteworthy that dopants for PCBM are usually incorporated through one-step solution processing, and, thus, the addition of dopants in the PCBM solution may also have beneficial effects on the morphological development of PCBM layers from the solution. It is shown that dopants such as GD[99] and oleamide[101] can improve the coverage and compactness of the solution-processed PCBM ETLs, contributing to the performance enhancements in PSCs. Therefore, the use of a dopant contributing to both, the intrinsic electronic properties and the morphologies of PCBM layers, can possibly lead to a further boost in the performance of PSCs.

4. Doping in HTLs

Like ETLs, HTLs can also be classified into two groups: organic and inorganic. So far, the most widely used HTL in PSCs is organic Spiro-OMeTAD molecules (the molecular structure is shown in Fig. 9C). However, due to the low hole mobility (~4×10^{-5} cm^2 V^{-1} s^{-1}) of the solution-processed Spiro-MeOTAD layer as result of a lack of molecular ordering, neat Spiro-OMeTAD is inadequate for achieving high PCEs in PSCs. In the past, a variety of materials have been reported as p-type dopants to enhance the electronic properties of the Spiro-OMeTAD layer for improved performance of solid-state DSSCs (see example in Fig. 9D). These dopants include $SnCl_4$,[102] $(p\text{-}BrC_6H_4)_3NSbCl_6$,[103] and tris(2-(1*H*-pyrazol-1-yl)pyridine)cobalt(III).[104] Lithium-bis-(trifluoromethylsulfonyl)-imide (Li-TFSI) salt has also been reported to enhance significantly the hole mobility of Spiro-OMeTAD, as Li^+ can react with oxygen and Spiro-OMeTAD to facilitate the formation of oxidized Spiro-OMeTAD, while the large anion $TFSI^-$ stabilizes the oxidized Spiro-OMeTAD.[105–108] For PSCs, the success of Li-TFSI dopant has been confirmed by the fact that most of the best PSCs employ a Spiro-OMeTAD layer with Li-TFSI doping. However, there are also issues associated with Li-TFSI due to its hydrophilic nature, which absorbs moisture from the ambient and degrades the PSCs. Therefore, other possible dopants have been explored. For example, Zhang *et al.*[109] reported an ionic liquid *N*-butyl-*N*′-(4-pyridylheptyl) imidazolium bis(trifluoro-methane)sulfonimide (BuPyIm-TFSI) in Spiro-OMeTAD, which can enhance both electronic properties and environmental stability.

Besides the most popular Spiro-OMeTAD HTL, a wide range of p-type semiconducting polymers are good HTL candidates for PSCs. Compared with Spiro-OMeTAD, these polymers usually have even poorer intrinsic electrical properties, in which case Li-TFSI is also added for their better function in the PSCs.[110] However, Heo *et al.*[111] suggested that those amine-moiety-free polymers do not form complexes with TFSI, where true chemical doping does not occur, and the significantly enhanced conductivity is due to the additional hole conduction mediated by Li-TFSI. Based on a similar mechanism, Xiao *et al.*[112] have shown that GD can also be a promising 'dopant' for polymer HTLs. For those organic HTLs generally used in inverted-structure PSCs,[113] less attention has been paid to doping, because either the applied HTL is already very conductive (*e.g.* poly(3,4-ethylenedioxythiophene) polystyrene sulfonate or PEDOT:PSS), or the thickness of the HTL can be small enough

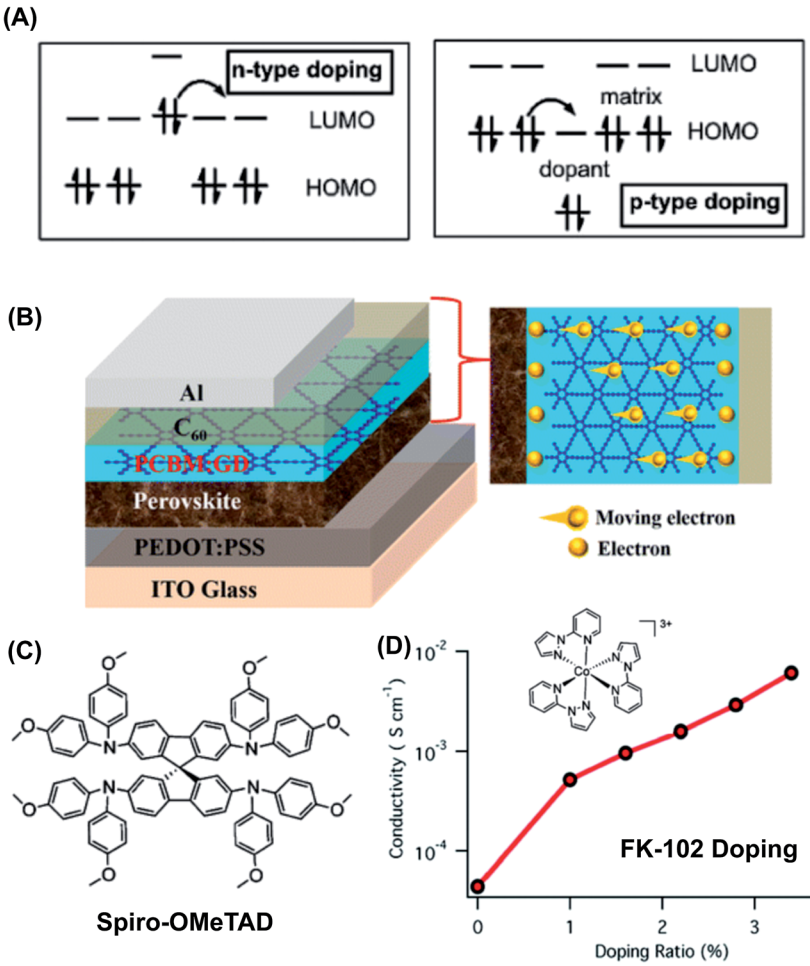

Fig. 9 (A) Schematic illustration of doping mechanism in organic semiconductors (reprinted with permission from ref. 96). (B) Schematic representation showing GD doping improving the electron mobility in PCBM in inverted-structure PSCs (reprinted with permission from ref. 99). (C) Molecular structure of Spiro-OMeTAD (reprinted with permission from ref. 104). (D) The doping effect of FK-102 (tris(2-(1*H*-pyrazol-1-yl) pyridine)cobalt(III)) on the conductivity of Spiro-OMeTAD HTL (reprinted with permission from ref. 104).

so that its conductivity does not limit the photocurrent extraction (*e.g.* poly(triaryl amine) poly[bis(4-phenyl)(2,4,6-trimethylphenyl)amine] or PTAA). For the latter, when a thicker PTAA layer is needed to smooth-out the substrate, doping of PTAA has also been explored with popular acceptors such as F4-TCNQ.[114]

Inorganic HTL materials, in particular NiO, have been studied extensively considering its higher stability and lower cost.[115–117] Similar to TiO_2, several metal ions can be used as dopants in NiO for enhancing its hole conduction.[118–121] In a recent PSC study, Chen *et al.*,[89] showed that through co-doping of NiO by Li and Mg (Fig. 8D), the conductivity can be increased to 2.32×10^{-3} S cm^{-1}, from 0.166×10^{-3} S cm^{-1} for an undoped NiO thin film. Also, Jung *et al.*[122] and Kim *et al.*[123] showed that Cu-doped NiO thin films can be an efficient HTL material for PSCs, highlighting the importance of doping in inorganic HTL materials. Like NiO, doping in other inorganic HTL materials such as CuI[124] and CuSCN[125] may have similar positive effects on PSCs performance, which has not been widely studied.

5. Doping in electrodes

At least one of the electrodes in PSCs needs to be transparent to allow sunlight into the device. Here doped transparent conductive oxide (TCO) are widely used, including fluorine-doped tin oxide (FTO) and indium-doped tin oxide (ITO). These two are commercially available, and are used as-received without further dopant engineering. However, the doping characteristics in this electrode could have several important implications on the PSC performance. First, the current FTO or ITO technology could be advanced further. The sheet resistance of commercially available FTO or ITO adds to the series resistance in PSCs, leading to a drop in the fill factor (FF) as the active area of the PSC increases.[126] Therefore, to explore more superior doping strategies to achieve highly transparent, conductive TCOs can play an important role in the fabrication of large-area PSC panels. Second, doping affects the E_F of the electrode, where the interfacial charge transfer characteristics can be influenced. Third, doping can also be used to engineer

the surface properties of TCOs, which can influence the growth of the ETL or HTL on top of the TCO layer.

6. Outlook

It is envisioned that future large-area PSCs are solution-processed at low temperatures, are high efficiency, and are highly durable. They are also expected to have various functionalities such as semitransparency, flexibility, and with tunable colors. Doping and alloying are two extremely important compositional engineering methods for meeting these desirable PSC characteristics. Indeed most recently reported state-of-the-art PSCs consist of layers that are doped and/or alloyed.[89,127,128] Thus, each functional layer in the future commercialized PSCs is likely to be doped and/or alloyed.

Although various doping and/or alloying strategies have been demonstrated to improve different aspects of PSCs in the literature, several challenges still remains in the fundamental understanding of the underlying mechanisms. First, the phase-homogeneity of these doped and/or alloyed layers (HOIP, HTL, ETL, and electrodes) awaits elucidation using high-spatial-resolution, high-sensitivity analytical characterization methods. Second, the exact role of doping and/or alloying in PSCs is difficult to elucidate, because doping and/or alloying can also influence the microstructural development of these solution-processed materials,[129] making it difficult to separate the different effects. Third, in the most important case of doping in HOIPs, many of studies in the literature have not justified the exact doping type (p or n), although the 'doping' effect has been claimed. This may be related to the fact that the p/i/n nature of PSCs themselves is still being debated. We believe that further advances in these fundamental aspects will point to clearer directions in the exploration of the most effective doping and/or alloying approaches that are important for the development of next-generation PSCs.

Acknowledgements

We thank the National Science Foundation (DMR-1305913 and OIA-1538893) for the financial support.

References

1 NREL Efficiency Chart, http://www.nrel.gov/ncpv/images/efficiency_chart.jpg.
2 A. Kojima, K. Teshima, Y. Shirai and T. Miyasaka, *J. Am. Chem. Soc.*, 2009, **131**, 6050–6051.
3 M. M. Lee, J. Teuscher, T. Miyasaka, T. N. Murakami and H. J. Snaith, *Science*, 2012, **338**, 643–647.
4 Y. Zhou and K. Zhu, *ACS Energy Lett.*, 2016, **1**, 64–67.
5 M. Liu, M. B. Johnston and H. J. Snaith, *Nature*, 2013, **501**, 395–398.
6 J. Burschka, N. Pellet, S.-J. Moon, R. Humphry-Baker, P. Gao, M. K. Nazeeruddin and M. Gräzel, *Nature*, 2013, **499**, 316–318.
7 P. V. Kamat, *J. Phys. Chem. Lett.*, 2015, **6**, 4874–4875.
8 Y. Kutes, L. Ye, Y. Zhou, S. Pang, B. D. Huey and N. P. Padture, *J. Phys. Chem. Lett.*, 2014, **5**, 3335–3339.
9 D. B. Mitzi, in *Progress in Inorganic Chemistry*, ed. K. D. Karlin, John Wiley & Sons, New York, 1999, vol. 48, pp. 1–122.
10 H.-S. Kim, C.-R. Lee, J.-H. Im, K.-B. Lee, T. Moehl, A. Marchioro, S.-J. Moon, R. Humphry-Baker, J.-H. Yum, J. E. Moser, M. Grätzel and N.-G. Park, *Sci. Rep.*, 2012, **2**, 591.
11 Y. Zhao and K. Zhu, *Chem. Soc. Rev.*, 2016, **45**, 655–689.
12 Y. Zhou, A. L. Vasiliev, W. Wu, M. Yang, S. Pang, K. Zhu and N. P. Padture, *J. Phys. Chem. Lett.*, 2015, **6**, 2292–2297.
13 N. J. Jeon, J. H. Noh, W. S. Yang, Y. C. Kim, S. Ryu, J. Seo and S. I. Seok, *Nature*, 2015, **517**, 476–480.
14 N. J. Jeon, J. H. Noh, Y. C. Kim, W. S. Yang, S. Ryu and S. I. Seok, *Nat. Mater.*, 2014, **13**, 897–903.
15 M. A. Green, A. Ho-Baillie and H. J. Snaith, *Nat. Photonics*, 2014, **8**, 506–514.
16 K. Miyano, N. Tripathi, M. Yanagida and Y. Shirai, *Acc. Chem. Res.*, 2016, **49**, 303–310.
17 C.-J. Jiang, M. Yang, Y. Zhou, B. To, S. U. Nanayakkara, J. M. Luther, W. Zhou, J. J. Berry, J. van de Lagemaat, N. P. Padture, K. Zhu and M. M. Al-Jassim, *Nat. Commun.*, 2015, **6**, 8397.
18 W. D. Callister and D. G. Rethwisch, *Materials Science and Engineering: An Introduction*, John Wiley & Sons, New York, 9th edn, 2015.
19 S. O. Kasap, *Principles of Electronic Materials and Devices*, McGraw Hill, New York, 3rd edn, 2006.
20 N. Andriotis and M. Menon, *J. Appl. Phys.*, 2015, **117**, 125708.
21 R. Barman, M. Motapothula, A. Annadi, K. Gopinadhan, Y. L. Zhao, Z. Yong, I. Santoso, Ariando, M. Breese, A. Rusydi, S. Dhar and T. Venkatesan, *Appl. Phys. Lett.*, 2011, **98**, 072111.
22 Y. Pei, N. A. Heinz and G. J. Snyder, *J. Mater. Chem.*, 2011, **21**, 18256–18260.
23 Y. Zhou, M. Yang, S. Pang, K. Zhu and N. P. Padture, *J. Am. Chem. Soc.*, 2016, **138**, 5535–5538.
24 N. Pellet, P. Gao, G. Gregori, T.-Y. Yang, M. K. Nazeeruddin, J. Maier and M. Grätzel, *Angew. Chem.*, 2014, **53**, 3151–3157.
25 A. Binek, F. C. Hanusch, P. Docampo and T. Bein, *J. Phys. Chem. Lett.*, 2015, **6**, 1249–1253.
26 C. C. Stoumpos, C. D. Malliakas and M. G. Kanatzidis, *Inorg. Chem.*, 2013, **52**, 9019–9038.
27 S. Pang, H. Hu, J. Zhang, S. Lv, Y. Yu, F. Wei, T. Qin, H. Xu, Z. Liu and G. Cui, *Chem. Mater.*, 2014, **26**, 1485–1491.
28 Z. Wang, Y. Zhou, S. Pang, Z. Xiao, J. Zhang, W. Chai, H. Xu, Z. Liu, N. P. Padture and G. Cui, *Chem. Mater.*, 2015, **27**, 7149–7155.
29 Y. Zhou, J. Kwun, H. F. Graces, S. Pang and N. P. Padture, *Chem. Comm.*, 2016, **52**, 7273–7275.
30 Y. Zhou, M. Yang, J. Kwun, O. S. Game, Y. Zhao, S. Pang, N. P. Padture and K. Zhu, *Nanoscale*, 2016, **8**, 6265–6270.
31 M. T. Waller, O. J. Weber, J. M. Frost and A. Walsh, *J. Phys. Chem. Lett.*, 2015, **6**, 3209–3212.
32 G. E. Eperon, C. E. Beck and H. J. Snaith, *Mater. Horiz.*, 2016, **3**, 63–71.

33 J. Liu, Y. Shirai, X. Yang, Y. Yue, W. Chen, Y. Wu, A. Islam and L. Han, *Adv. Mater.*, 2015, **27**, 4918–4923.
34 Y. Deng, Q. Dong, C. Bi, Y. Yuan and J. Huang, *Adv. Energy Mater.*, 2016, **6**, 1600372.
35 J.-W. Lee, D.-H. Kim, H.-S. Kim, S.-W. Seo, S. M. Cho and N.-G. Park, *Adv. Energy Mater.*, 2015, **5**, 1501310.
36 C. Yi, J. Luo, S. Meloni, A. Boziki, N. Ashari-Astani, C. Grätzel, S. M. Zakeeruddin, U. Röthlisberger and M. Grätzel, *Energy Environ. Sci.*, 2016, **9**, 656–662.
37 Z. Li, M. Yang, J.-S. Park, S.-H. Wei, J. J. Berry and K. Zhu, *Chem. Mater.*, 2016, **28**, 284–292.
38 N. Wang, Y. Zhou, M.-G. Ju, H. F. Graces, T. Ding, S. Pang, X. C. Zeng, N. P. Padture and X. W. Sun, *Adv. Energy Mater.*, 2016, DOI: 10.1002/aenm.201601130, in press.
39 N. K. Noel, S. D. Stranks, A. Abate, C. Wehrenfenning, S. Guarnera, A. Haghighirad, A. Sadhanala, G. E. Eperon, S. K. Pathak, M. B. Johnston, A. Petrozza, L. M. Herz and H. J. Snaith, *Energy Environ. Sci.*, 2014, **7**, 3061–3068.
40 F. Hao, C. C. Stoumpos, D. H. Cao, R. P. H. Chang and M. G. Kanatzidis, *Nat. Photonics*, 2014, **8**, 489–494.
41 F. Hao, C. C. Stoumpos, R. P. H. Chang and M. G. Kanatzidis, *J. Am. Chem. Soc.*, 2014, **136**, 8094–8099.
42 Y. Ogomi, A. Morita, S. Tsukamoto, T. Saitho, N. Fujikawa, Q. Shen, T. Toyoda, K. Yoshino, S. S. Pandey, T. Ma and S. Hayase, *J. Phys. Chem. Lett.*, 2014, **5**, 1004–1011.
43 A. Babayigit, D. D. Thanh, A. Ethirajan, J. Manca, M. Muller, H.-G. Boyen and B. Conings, *Sci. Rep.*, 2016, **6**, 18721.
44 A. Babayigit, A. Ethirajan, M. Marc and B. Coning, *Nat. Mater.*, 2016, **15**, 247–251.
45 M.-G. Ju, G. Sun, Y. Zhao and W. Liang, *Phys. Chem. Chem. Phys.*, 2015, **17**, 17679–17687.
46 E. Mosconi, P. Umari and F. D. Angelis, *J. Mater. Chem. A*, 2015, **3**, 9208–9215.
47 A. Mancini, P. Quadrelli, C. Milanese, M. Patrini, G. Guizzetti and L. Malavasi, *Inorg. Chem.*, 2015, **54**, 8893–8895.
48 *Organic-Inorganic Halide Perovskite Photovoltaics: From Fundamentals to Device Architecture*, ed. N.-G. Park, M. Grätzel and T. Miyasaka, Springer, Switzerland, 2016.
49 K. T. Butler, J. M. Frost and A. Walsh, *Mater. Horiz.*, 2015, **2**, 228–231.
50 J. H. Noh, S. H. Im, J. H. Heo, T. N. Mandal and S. I. Seok, *Nano Lett.*, 2013, **13**, 1764–1769.
51 Y. Zhou, M. Yang, O. S. Game, W. Wu, J. Kwun, M. A. Strauss, Y. Yan, J. Huang, K. Zhu and N. P. Padture, *ACS Appl. Mater. Interfaces*, 2016, **8**, 2232–2237.
52 C. D. Bailie, M. G. Christoforo, J. P. Mailoa, A. R. Boweing, E. L. Unger, W. H. Nguyen, J. Burschka, N. Pellet, J. Z. Lee, M. Gräztel, R. Noufi, T. Buonassisi, A. Salleo and M. D. McGehee, *Energy Environ. Sci.*, 2015, **8**, 956–963.
53 E. T. Hoke, D. J. Slotcavage, E. R. Dohner, A. R. Bowring, H. I. Karunadasa and M. D. McGehee, *Chem. Sci.*, 2015, **6**, 613–617.
54 D. P. McMeekin, G. Sadoughi, W. Rehman, G. E. Eperon, M. Saliba, M. T. Höranter, A. Haghighirad, N. Sakai, L. Korte, B. Rech, M. B. Johnston, L. M. Herz and H. J. Snaith, *Science*, 2016, **351**, 151–155.
55 R. K. Misra, L. Ciammaruchi, S. Aharon, D. Mogilyansky, L. Etgar, I. Visoly-Fisher and E. A. Katz, *ChemSusChem*, 2016, **9**, 1–7.
56 X. Li, D. Bi, C. Yi, J.-D. Décoppet, J. Luo, S. M. Zakeeruddin, A. Hagfeldt and M. Gräztel, *Science*, 2016, **353**, 58–62.
57 J. P. C. Baena, L. Sterier, W. Tress, M. Saliba, S. Neutzner, T. Matsui, F. Giordano, T. J. Jacobsson, A. R. S. Kandada, S. M. Zakeeruddin, A. Petrozza, A. Abate, M. K. Nazeeruddin, M. Grätzel and A. Hagfeldt, *Energy Environ. Sci.*, 2015, **8**, 2928–2934.
58 D. Bi, W. Tress, M. I. Dar, P. Gao, J. Luo, C. Renevier, K. Schenk, A. Abate, F. Giordano, J.-P. C. Baena, J.-D. Desoppet, S. M. Zakeeruddin, M. K. Nazeeruddin, M. Grätzel and A. Hagfeldt, *Sci. Adv.*, 2016, **2**, 1–7.
59 M. Saliba, T. Matsui, J.-y. Seo, K. Domanski, J.-P. Correa-Baena, M. K. Nazeeruddin, S. M. Zakeeruddin, W. Tress, A. Abate, A. Hagfeldt and M. Grätzel, *Energy Environ. Sci.*, 2016, **9**, 1989–1997.
60 T. J. Jacobsson, J. Correa-Baena, M. Pazoki, M. Saliba, K. Schenk, M. Grätzel and A. Hagfeldt, *Energy Environ. Sci.*, 2016, **9**, 1706–1724.
61 M. Grätzel, *Nat. Mater.*, 2014, **13**, 838–842.
62 S. Colella, E. Mosconi, P. Fedeli, A. Listorti, F. Gazza, F. Orlandi, P. Ferro, T. Besagni, A. Rizzo, G. Calestani, G. Gigli, F. D. Angelis and R. Mosca, *Chem. Mater.*, 2013, **25**, 4613–4618.
63 S. Colella, E. Mosconi, G. Pellegrino, A. Alberti, V. L. P. Guerra, S. Masi, A. Listorti, A. Rizzo, G. G. Condorelli, F. D. Angelis and G. Gigli, *J. Phys. Chem. Lett.*, 2014, **5**, 3532–3538.
64 D. W. deQuilettes, S. M. Vorpahl, S. D. Stranks, H. Nagaoka, G. E. Eperon, M. E. Ziffer, H. J. Snaith and D. S. Ginger, *Science*, 2015, **348**, 683–686.
65 H. Yu, F. Wang, F. Xie, W. Li, J. Chen and N. Zhao, *Adv. Funct. Mater.*, 2014, **24**, 7102–7108.
66 Q. Dong, Y. Yuan, Y. Shao, Y. Fang, Q. Wang and J. Huang, *Energy Environ. Sci.*, 2015, **8**, 2464–2470.
67 Y. Zhao and K. Zhu, *J. Phys. Chem. C*, 2014, **118**, 9412–9418.
68 A. L. Abdelhady, M. I. Saidaminov, B. Murali, V. Adinolfi, O. Voznyy, K. Katsiev, E. Alarousu, R. Comin, I. Dursun, L. Sinatra, E. H. Sargent, O. F. M. Ohammed and O. M. Bakr, *J. Phys. Chem. Lett.*, 2016, **7**, 295–301.
69 J. Chen, Y. Rong, A. Mei, Y. Xiong, T. Liu, Y. Sheng, P. Jiang, L. Hong, Y. Guan, X. Zhu, X. Hou, M. Duan, J. Zhao, X. Li and H. Han, *Adv. Energy Mater.*, 2016, **6**, 1502009.
70 A. Halder, R. Chulliyil, A. S. Subbiah, T. Khan, S. Chattoraj, A. Chowdhury and S. K. Sarkar, *J. Phys. Chem. Lett.*, 2015, **6**, 3483–3489.
71 M. Abdi-Jalebi, M. I. Dar, A. Sadhanala, S. P. Senanayak, M. Franckvičius, N. Arora, Y. Hu, M. K. Nazeeruddin, S. M. Zakeeruddin, M. Grätzel and R. H. Friend, *Adv. Energy Mater.*, 2016, **6**, 1502472.
72 A. Mei, X. Li, L. Liu, Z. Ku, T. Liu, Y. Rong, M. Xu, M. Hu, J. Chen, Y. Yang, M. Grätzel and H. Han, *Science*, 2014, **345**, 295–298.
73 Q. Tai, P. You, H. Sang, Z. Liu, C. Hu, H. L. W. Chan and F. Yan, *Nat. Commun.*, 2016, **7**, 11105.

74 J. T.-W. Wang, Z. Wang, S. Pathak, W. Zhang, D. W. deQuilettes, F. Wisnivesky-Rocca-Rivarola, J. Huang, P. K. Nayak, J. B. Patel, H. A. M. Yusof, Y. Vanzof, R. Zhu, I. Ramirez, J. Zhang, C. Ducati, C. Grovenor, M. B. Johnston, D. S. Ginger, R. J. Nicholas and H. J. Snaith, *Energy Environ. Sci.*, 2016, **9**, 2892–2901.
75 W.-J. Yin, T. Shi and Y. Yan, *Appl. Phys. Lett.*, 2014, **104**, 063903.
76 Q. Wang, Y. Shao, H. Xie, L. Lyu, X. Liu, Y. Gao and J. Huang, *Appl. Phys. Lett.*, 2014, **105**, 163508.
77 W. Zhang, G. E. Eperon and H. J. Snaith, *Nature Energy*, 2016, **1**, 16048.
78 C. S. Ponseca, T. J. Savenije, M. Abdellah, K. Zhang, A. Yarsev, T. Pascher, T. Harlang, P. Chabera, T. Pullerits, A. Stepanov, J.-P. Wolf and V. Sundström, *J. Am. Chem. Soc.*, 2014, **136**, 5189–5192.
79 B. Roose, S. Pathak and U. Steiner, *Chem. Soc. Rev.*, 2015, **44**, 8326–8349.
80 K. H. Ko, Y. C. Lee and Y. J. Jung, *J. Colloid Interface Sci.*, 2005, **283**, 482–487.
81 F. Fabregat-Santiago, E. M. Barea, J. Bisquert, G. K. Mor, K. Shankar and C. A. Grimes, *J. Am. Chem. Soc.*, 2008, **130**, 11312–11316.
82 S. Lee, J. H. Noh, H. S. Han, D. K. Yim, D. H. Kim, J.-H. Lee, J. Y. Kim, H. S. Jung and K. S. Hong, *J. Phys. Chem. C*, 2009, **113**, 6878–6882.
83 J. Wang, M. Qin, H. Tao, W. Ke, Z. Chen, J. Wan, P. Qin, L. Xiong, H. Lei, H. Yu and G. Fang, *Appl. Phys. Lett.*, 2015, **106**, 121104.
84 D. H. Kim, G. S. Han, W. M. Seong, J.-W. Lee, B. J. Kim, N.-G. Park, K. S. Hong, S. Lee and H. S. Jung, *ChemSusChem*, 2015, **8**, 2392–2398.
85 T. Oku, T. Iwata and A. Suzuki, *Chem. Lett.*, 2015, **44**, 1033–1035.
86 B.-X. Chen, H.-S. Rao, W.-G. Li, Y.-F. Xu, H.-Y. Chen, D.-B. Kuang and C.-Y. Su, *J. Mater. Chem. A*, 2016, **4**, 5647–5653.
87 Y. Ogomi, K. Kukihara, S. Qing, T. Toyoda, K. Yoshino, S. Pandey, H. Momose and S. Hayase, *ChemPhysChem*, 2014, **15**, 1062–1069.
88 H. Zhou, Q. Chen, G. Li, S. Luo, T.-B. Song, H.-S. Duan, Z. Hong, J. You, Y. Liu and Y. Yang, *Science*, 2014, **345**, 542–546.
89 W. Chen, Y. Wu, Y. Yue, J. Liu, W. Zhang, X. Yang, H. Chan, E. Bi, I. Ashraful, M. Grätzel and L. Han, *Science*, 2015, **350**, 944–948.
90 S. K. Pathak, A. Abate, P. Ruckdeschel, B. Roose, K. C. Gödel, Y. Vaynzof, A. Santhala, S.-I. Watanabe, D. J. Hollman, N. Noel, A. Sepe, U. Wiesner, R. Friend, H. J. Snaith and U. Striner, *Adv. Funct. Mater.*, 2014, **24**, 6046–6055.
91 H. Nagaoka, F. Ma, D. W. deQuilettes, S. M. Vorpahl, M. S. Glaz, A. E. Colbert, M. E. Ziffer and D. S. Ginger, *J. Phys. Chem. Lett.*, 2015, **6**, 669–675.
92 F. Giordano, A. Abate, J. P. C. Baena, M. Saliba, T. Matsui, J. Seo, K. Domanski, J. Correa-Baena, M. K. Nazeeruddin, S. M. Zakeeruddin, W. Tress, A. Abate, A. Hagfeldt and M. Grätzel, *Energy Environ. Sci.*, 2016, **9**, 1989–1997.
93 P. Qin, A. L. Domanski, A. K. Chandiran, R. Berger, H.-J. Butt, M. I. Dar, T. Moehl, N. Tetreault, P. Gao, S. Ahmad, M. K. Nazeeruddin and M. Gräztel, *Nanoscale*, 2014, **6**, 1508–1514.
94 B. Lüssem, M. Riede and K. Leo, *Phys. Status Solidi A*, 2013, **210**, 9–43.
95 M. Sygletou, G. Kakavelakis, B. Paci, A. Generosi, E. Kymakis and E. Stratakis, *ACS Appl. Mater. Interfaces*, 2015, **7**, 17756–17764.
96 K. Walzer, B. Maennig, M. Pfeiffer and K. Leo, *Chem. Rev.*, 2007, **107**, 1233–1271.
97 A. Armin, G. Juska, B. W. Philippa, P. L. Burn, P. Meredith, R. D. White and A. Pivrikas, *Adv. Energy. Mater.*, 2013, **3**, 321–327.
98 S. S. Kim, S. Bae and W. H. Jo, *Chem. Commun.*, 2015, **51**, 17413–17416.
99 C. Kuang, G. Tang, T. Jiu, H. Yang, H. Liu, B. Liu, W. Luo, X. Li, W. Zhang, F. Lu, J. Fang and Y. Li, *Nano Lett.*, 2015, **15**, 2756–2762.
100 Y. Bai, Q. Dong, Y. Shao, Y. Deng, Q. Wang, L. Shen, D. Wang, W. Wei and J. Huang, *Nat. Commun.*, 2016, **7**, 21806.
101 F. Xia, Q. Wu, P. Zhou, Y. Li, X. Chen, Q. Liu, J. Zhu, S. Dai, Y. Lu and S. Yang, *ACS Appl. Mater. Interfaces*, 2015, **7**, 13659–13665.
102 M. Xu, Y. Rong, Z. Ku and H. Han, *J. Phys. Chem. C*, 2013, **117**, 22492–22496.
103 U. Bach, D. Lupo, P. Comte, J. E. Moser, F. Weissörtel, J. Salbeck, H. Spreitzar and M. Grätzel, *Nature*, 1998, **359**, 583–585.
104 J. Burschka, A. Dualeh, F. Kessler, E. Baranoff, N. Cevey-Ha, C. Yi, M. K. Nazeeruddin and M. Grätzel, *J. Am. Chem. Soc.*, 2011, **133**, 18042–18045.
105 S. Wang, W. Yuan and Y. S. Meng, *ACS Appl. Mater. Interfaces*, 2015, **7**, 24791–24798.
106 W. H. Nguyen, C. D. Bailie, E. L. Unger and M. D. McGehee, *J. Am. Chem. Soc.*, 2014, **136**, 10996–11001.
107 J. H. Noh, N. J. Jeon, Y. C. Choi, M. K. Nazeeruddin, M. Grätzel and S. I. Seok, *J. Mater. Chem. A*, 2013, **1**, 11842–11847.
108 A. Abate, T. Leijtens, S. Pathak, J. Teuscher, R. Avolio, M. E. Errico, J. Kirkpatrik, J. M. Ball, P. Docampo, I. McPherson and H. J. Snaith, *Phys. Chem. Chem. Phys.*, 2013, **15**, 2572–2579.
109 H. Zhang, Y. Shi, F. Yan, L. Wang, K. Wang, Y. Xing, Q. Dong and T. Ma, *Chem. Commun.*, 2014, **50**, 5020–5022.
110 J. H. Heo, S. H. Im, J. H. Noh, T. N. Mandal, C. Lim, J. A. Chang, Y. H. Lee, H. Kim, A. Sarkar, M. K. Nazeeruddin, M. Grätzel and S. I. Seok, *Nat. Photonics*, 2013, **7**, 486–491.
111 J. H. Heo and S. H. Im, *Phys. Status Solidi RRL*, 2014, **8**, 816–821.
112 J. Xiao, J. Shi, H. Liu, Y. Xu, S. Lv, Y. Luo, D. Li, Q. Meng and Y. Li, *Adv. Energy Mater.*, 2015, **5**, 1401943.

113 T. Liu, K. Chen, Q. Hu, R. Zhu and Q. Gong, *Adv. Energy Mater.*, 2016, **6**, 1600457.
114 Q. Wang, C. Bi and J. Huang, *Nano Energy*, 2015, **15**, 275–280.
115 J. H. Park, J. Seo, S. Park, S. S. Shin, Y. C. Kim, N. J. Jeon, H.-W. Shin, T. K. Ahn, J. H. Noh, S. C. Yoon, C. S. Hwang and S. I. Seok, *Adv. Mater.*, 2015, **27**, 4013–4019.
116 J. You, L. Meng, T.-B. Song, T.-F. Guo, Y. M. Yang, W.-H. Chang, Z. Hong, H. Chen, H. Zhou, Q. Chen, Y. Liu, N. D. Marco and Y. Yang, *Nat. Nanotechnol.*, 2016, **11**, 75–81.
117 X. Xu, Z. Liu, Z. Zuo, M. Zhang, Z. Zhao, Y. Shen, H. Zhou, Q. Chen, Y. Yang and M. Wang, *Nano Lett.*, 2015, **15**, 2402–2408.
118 S. Tong, M. Zheng, Y. Lu, Z. Lin, J. Li, X. Zhang, Y. Shi, P. He and H. Zhou, *J. Mater. Chem. A*, 2015, **3**, 16177–16182.
119 X. Y. Sun, B. Li and H. Metiu, *J. Phys. Chem. C*, 2013, **117**, 23597–23608.
120 K. Matsubara, S. Huang, M. Iwamoto and W. Pan, *Nanoscale*, 2014, **6**, 688–692.
121 K. Vallaperuman, M. Parthibavarman, S. Sathishkumar, M. Durairaj and K. Thavamani, *Korean J. Chem. Eng.*, 2014, **31**, 639–643.
122 J. W. Jung, C. Chueh and A. K.-Y. Jen, *Adv. Mater.*, 2015, **27**, 7874–7880.
123 J. H. Kim, P. W. Liang, S. T. Williams, N. Cho, C. Chueh, M. S. Glaz, D. S. Ginger and A. K.-Y. Jen, *Adv. Mater.*, 2015, **27**, 695–701.
124 J. A. Christians, R. C. M. Fung and P. V. Kamat, *J. Am. Chem. Soc.*, 2014, **136**, 758–764.
125 P. Qin, S. Tanaka, S. Ito, N. Tetreault, K. Manabe, H. Nishino, M. K. Nazeeruddin and M. Grätzel, *Nat. Commun.*, 2014, **5**, 3834.
126 M. Yang, Y. Zhou, Y. Zeng, C. Jiang, N. P. Padture and K. Zhu, *Adv. Mater.*, 2015, **27**, 6363–6370.
127 G. E. Eperon, T. Leijtens, K. A. Bush, R. Prasanna, T. Green, J. T.-W. Wang, D. P. McMeekin, G. Volonakis, R. L. Milot, R. May, A. Palmstrom, D. J. Slotcavage, R. A. Belisle, J. B. Patel, E. S. Parrott, R. J. Sutton, W. Ma, F. Moghadam, B. Conings, A. Babayigit, L. M. Herz, M. B. Johnston, M. D. McGehee and H. J. Snaith, *Science*, 2016, DOI: 10.1126/science.aaf9717, in press.
128 M. Saliba, T. Matsui, K. Domanski, J.-K. Seo, A. Ummadisingu, S. M. Zakeeruddin, J.-P. Correa-Baena, W. R. Tress, A. Abate, A. Hagfeldt and M. Grätzel, *Science*, 2016, **354**, 206–209.
129 Y. Zhou, O. S. Game, S. Pang and N. P. Padture, *J. Phys. Chem. Lett.*, 2015, **6**, 4827–4839.